Optik - International Journal for Light and Electron Optics 247 (2021) 167868

Contents lists available at ScienceDirect

Optik

journal homepage: www.elsevier.com/locate/ijleo

Power flow in multimode step-index plastic photonic crystal fibers

Svetislav Savović [a,b,*], Milan S. Kovačević [a], Branko Drljača [c], Ana Simović [a], Ljubica Kuzmanović [a], Alexandar Djordjevich [b]

[a] University of Kragujevac, Faculty of Science, Kragujevac, Serbia
[b] City University of Hong Kong, Department of Mechanical Engineering, Hong Kong, China
[c] University of Priština in Kosovska Mitrovica, Faculty of Sciences and Mathematics, L. Ribara 29, Kosovska Mitrovica, Serbia

ARTICLE INFO

Keywords:
photonic crystal fiber
step-index fiber
power flow equation
coupling lengths

ABSTRACT

We investigate the state of mode coupling in a multimode step-index plastic photonic crystal fiber (SI PPCF) with a solid-core by solving the time-independent power flow equation. For various arrangements of air-holes, and therefore a different numerical apertures (NAs), as well as a different widths of launch beam distribution, the length L_c for achieving equilibrium mode distribution (EMD) and length z_s at which a steady state distribution (SSD) is established are determined for such fiber. We show that the larger the air holes in the cladding (higher NA), the longer length of the fiber it takes for the modal distribution-transients to reach their equilibrium and steady state. This is as a consequence of the greater participation rate of higher-order modes in higher-aperture photonic-crystal fibers. In contrary, in the case of a wide launch that excites more guiding modes, these lengths shorten. This is because the energy of a wide launch beam is more uniformly distributed among guided modes in the fiber, thus the EMD and SSD are reached at shorter distances than for a narrow launch beam. Such information is of interest for application of multimode photonic crystal fibers in telecommunication and fiber optic sensors.

* Correspondence to: Faculty of Science, R. Domanovića 12, 34000 Kragujevac, Serbia.
E-mail address: savovic@kg.ac.rs (S. Savović).

https://doi.org/10.1016/j.ijleo.2021.167868
Received 30 June 2021; Received in revised form 18 August 2021; Accepted 20 August 2021
Available online 21 August 2021

provides additional versatility to affect its sectional profile during the design stage. For example, “endlessly single-mode” PCFs that operate in only the fundamental mode across a broad wavelength range have been defined [2]. A PCF, on the other hand, may have a hollow core.The hollow fiber’s "air center" can have a lower refractive index than the cladding material [12,13] thanks to photonic bandgap guidance [8–11]. Dispersion [14–16], birefringence [17], supercontinuum generation [18–20], wavelength conversion [21, 22], optofluidics [23], and sensing [24] are just a few of the many recorded applications of PCFs.

The numerical aperture, NA, of the PCF is determined by the width of the material between holes in the cladding. The impracticality of cleaving fibers with even larger NAs having big holes and little material remaining between [25–27] appears to limit it to NA $\simeq$ 0.5–0.6. A heavy metal-oxide glass fiber [28] or a hollow core fiber filled with liquid [29] are two examples of PCFs to consider. Lensless focusing with excellent resolution has been registered with high NA PCFs [30].

Differential mode attenuation, mode coupling, and modal dispersion all affect PCF propagation characteristics. Mode coupling is primarily caused by light scattering that transfers power from one mode to another in multimode optical fibers due to intrinsic perturbations. Various irregularities, such as microscopic bends, voids and cracks and density variations, can cause these effects. The length-dependent variations of pulse dispersion and bandwidth are caused by mode coupling effects. We calculated spatial transients of power distribution and characteristic lengths at which EMD and SSD are achieved for different widths of launch beam distribution for multimode SI PPCF with solid core and three different diameters of air-holes in the cladding (three different NAs) for multimode SI

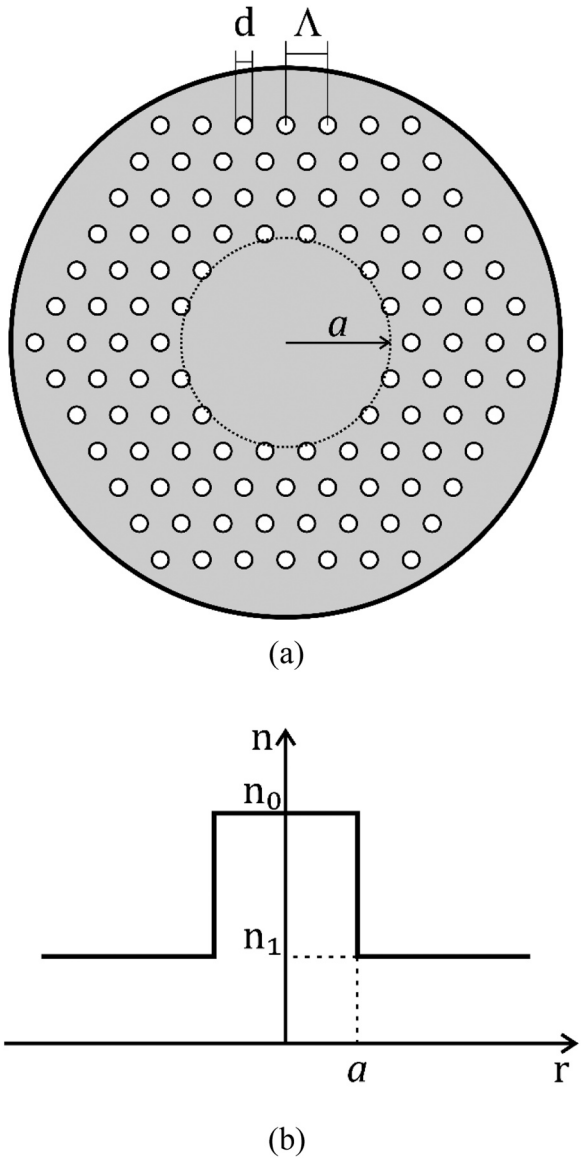

Fig. 1. (a) Cross section of multimode SI PCF with a solid-core and rings of air holes in the cladding, where Λ is the hole-to-hole spacing (pitch), d is diameter of air holes in the cladding, white area indicates air holes, (b) refractive-index profile of the referent multimode SI PPCF.

PPCF with solid core. The cladding holes are set in a triangular pattern with a constant pitch (see Fig. 1). We used the explicit finite differences method (EFDM) to solve the time-independent power flow equation for such a fiber. The parametric variance of the size of air-holes and the width of the launch beam distribution has an effect on characteristic coupling lengths, as shown in the Numerical Results.

2. SI PPCF design

Over the SI PPCF cladding, air-holes are usually uniform in size and form a regular triangular lattice. Where the size (d) or pitch (spacing density) (Λ) of the cladding layer could be changed to achieve the desired effective refractive index. Additional design parameters, such as air-hole spacing and size, are used to monitor numerical aperture, dispersion, and other fiber properties (Fig. 1). Despite uniform material properties in the fiber, the central part without holes has the highest refractive index n_0; holes in the cladding decrease the effective value n_1 of such index; larger or more densely spaced holes in the cladding further reduce it.

3. Time-independent power flow equation

The power flow in multimode SI optical fibers can be represented by the Gloge's time- independent power flow equation [31].

$$\frac{\partial P(\theta,z)}{\partial z} = -\alpha(\theta)P\left(\theta,z\right)+\frac{D}{\theta}\frac{\partial}{\partial\theta}\left(\theta\frac{\partial P(\theta,z)}{\partial\theta}\right) \tag{1}$$

where $P(\theta,z)$ is the angular power distribution at distance z from the input end of the fiber, θ is the propagation angle with respect to the core axis, D is the coupling coefficient assumed constant [31,32], and $\alpha(\theta)$is the modal attenuation (except near cutoff, the attenuation remains uniform $\alpha(\theta)=\alpha_0$ throughout the region of guided modes $0\le\theta\le\theta_m$) [33]. The boundary conditions are $\partial P(\theta_m,z)=0$ and $D(\partial P/\partial\theta)|_{\theta=0}=0$, where $\theta_m$is the maximum propagation angle (critical angle).

In order to apply the EFDM, we express Eq. (1) in the following form:

$$\frac{\partial P(\theta,z)}{\partial z} = -\alpha_0 P\left(\theta,z\right)+\frac{D}{\theta}\frac{\partial P(\theta,z)}{\partial\theta}+D\frac{\partial^2 P(\theta,z)}{\partial\theta^2} \tag{2}$$

We used the central difference scheme to represent the $(\partial P(\theta,z))/\partial\theta$ and $(\partial^2 P(\theta,z))/\partial\theta^2$ terms, and the forward difference scheme for the derivative term $(\partial P(\theta,z))/\partial z$. Then, Eq. (2) reads:

$$P_{i,j+1}=\left(\frac{\Delta zD}{\Delta\theta^2}-\frac{\Delta zD}{2\theta_{i,j}\Delta\theta}\right)P_{i-1,j}+\left(1-\frac{2\Delta zD}{\Delta\theta^2}-\Delta z\alpha_0\right)P_{i,j}+\left(\frac{\Delta zD}{2\theta_{i,j}\Delta\theta}+\frac{\Delta zD}{\Delta\theta^2}\right)P_{i+1,j} \tag{3}$$

where indexes i and j refer to the discrete step lengths $\Delta\theta$ and Δz for the angle θ and length z, respectively. This is a simple formula for $P_{i,j+1}$ at the $(i,j+1)^{\text{th}}$ mesh point in terms of the known values along the j^{th} distance row. The truncation error for the difference Eq. (3) is $O(\Delta z,\Delta\theta^2)$. In the difference form, the boundary conditions can be expressed as $P_{N,j}=0;\quad P_{0,j}=P_{1,j}$, where $N=(\theta_m/\Delta\theta)$ is grid dimension in the θ direction.

4. Numerical results

In a multimode solid-core SI PPCF, we investigated spatial transients of power distribution as well as an EMD and SSD for different widths of launch beam distribution. The effective refractive index of cladding n_{fsm} for SI PPCFs with air holes in a triangular lattice can be calculated using the effective parameter:

$$V=\frac{2\pi}{\lambda}a_{eff}\sqrt{n_0^2-n_{fsm}^2} \tag{4}$$

where n_0 is the refractive index of the core. The cladding's effective refractive index $n_{fsm}$is defined as the effective refractive index of so-

Table 1
Fitting coefficients in Eq. (6).

	$i=1$	$i=2$	$i=3$	.
a_{i0}	0.54808	0.71041	0.16904	-1.52736
a_{i1}	5.00401	9.73491	1.85765	1.06745
a_{i2}	-10.43248	47.41496	18.96849	1.93229
a_{i3}	8.22992	-43750962	-42.4318	3.89
b_{i1}	5	1.8	1.7	-0.84
b_{i2}	7	7.32	10	1.02
b_{i3}	9	22.8	14	13.4

called fundamental space-filling mode in the triangular hole lattice, and $a_{eff} = \Lambda/\sqrt{3}$ [34]. The effective refractive index of the cladding $n_1 \equiv n_{fsm}$, can be obtained from Eq. (4), using the effective V parameter [34]:

$$V\left(\frac{\lambda}{\Lambda}, \frac{d}{\Lambda}\right) = A_1 + \frac{A_2}{1 + A_3 \exp(A_4 \lambda/\Lambda)} \tag{5}$$

with the fitting parameters A_i ($i = 1$ to 4):

$$A_i = a_{i0} + a_{i1}\left(\frac{d}{\Lambda}\right)^{b_{i1}} + a_{i2}\left(\frac{d}{\Lambda}\right)^{b_{i2}} + a_{i3}\left(\frac{d}{\Lambda}\right)^{b_{i3}} \tag{6}$$

where the coefficients a_{i0} to a_{i3} and b_{i1} to b_{i3} ($i = 1$ to 4) are given in Table 1.

Fig. 2 depicts the effective refractive index of the cladding $n_1 \equiv n_{fsm}$ as a function of λ/Λ, for $\Lambda = 3$ μmand for three different values of the hole diameter of the cladding $d = 1$ μm, 1.5 μm and 2 μm. Relevant values of the effective refractive index n_1, relative refractive index difference Δ, air-hole diameters of the cladding d, and critical angles θ_m, are summarized in Table 2 for the operating wavelength of light of 645 nm.

The time-independent power flow Eq. (2) was solved using the EFDM for the multimode SI PPCF with solid core with $n_0 = 1.492$, core diameter $2a = 0.980$ mm, fiber diameter $b = 1$ mm, $D = 1.649 \times 10^{-4}$ rad^2/m and $\alpha_0 = 0.22$ dB/m (typical value of D and α_0 for standard POFs [33]). One should note that in modeling the SI PPCF one can use the typical values of D which characterizes a standard SI POF, since a strength of mode coupling in both types of plastic optical fibers is related to the plastic core material. Namely, mode coupling in both types of optical fibers is mainly caused by light scattering that transfers power from one mode to another due to various irregularities in plastic core, such as microscopic bends, voids, cracks and density variations. A similar assumption has been made in modeling a silica W-type PCF [35]. One should note that for bent POFs mode coupling is much stronger [36], which is expected to happen in bent PPCFs too. In order to look at the impact of the diameter of the air holes in the cladding (i.e. the influence of NA of the fiber) on the power distribution, we analyzed cases with diameter of air holes in the cladding $d = 1$ μm, 1.5 μm and 2 μm and launch beam distribution with $(\text{FWHM})_{z=0} = 1°$, 5 ° and 10°. As illustration, Fig. 3 shows the evolution of the normalized output angular power distribution with fiber length for the case with $d = 2$ μm calculated for Gaussian launch beam distributions with $(\text{FWHM})_{z=0} = 5°$. It can be seen from Fig. 3 that when the Gaussian launch beam distribution at the input end of the fiber is centered at $\theta_0 = 0°$, the distribution of the power remains at the same angle as the distance from the input fiber end increases. However, due to mode coupling, its width increases. In short fibers, the radiation patterns of non-centrally launched beams are positioned at values similar to their initial values. With increasing the fiber length one can observe that coupling is stronger for the low-order modes: their distributions have shifted more towards $\theta = 0°$. Coupling of higher-order modes can be observed only after longer fiber lengths. It is not until the fiber's coupling length L_c that all the mode-distributions shift their mid-points to zero degrees (from the initial value of θ_0 at the input fiber end), producing the EMD at fiber length $z = L_c = 39$ m and the SSD at length z = z_s= 102 m. Length z_s marks the fiber length where the output angular power distribution becomes completely independent on the launch beam distribution. The lengths L_c and z_s increase with the air-hole size (diameter d), that relates to the increase of NA of the multimode SI PPCF (Table 3). This is due to the higher participation rate of higher-order modes in photonic crystal fibers with larger numerical apertures. In contrary, the wider the launch beam, the shorter the length at which EMD and SSD are established (Figs. 4 and 5). This is due to the energy of a wide launch beam which is more uniformly distributed among guided modes in the fiber, that forces the EMD and SSD at shorter distances than for a narrow launch beam.

The results reported in this work can be used in employing the PPCFs as a part of various sensory systems [37] and compare their performance with standard POF sensors [38]. On the other hand, the mode coupling behavior determines the length dependence of the

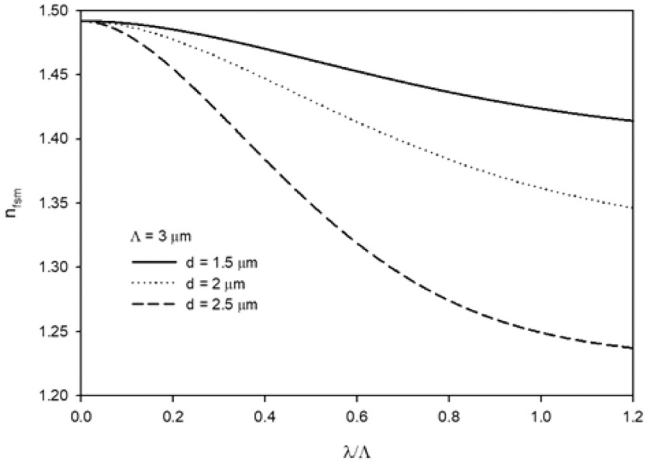

Fig. 2. Effective refractive index of the inner cladding as a function of λ/Λ.

Table 2
Effective refractive index of the cladding n_1, relative refractive index difference $\Delta = (n_0 - n_1)/n_0$, where $n_0 = 1.492$, and the critical angle θ_m for varied air-hole diameter d (wavelength: 645 nm).

d (μm)	1.0	1.5	2.0
n_1	1.4844	1.4757	1.4458
$\Delta = (n_0 - n_1)/n_0$	0.673673	0.677645	0.691611
θ_m (deg.)	5.79	8.48	14.28

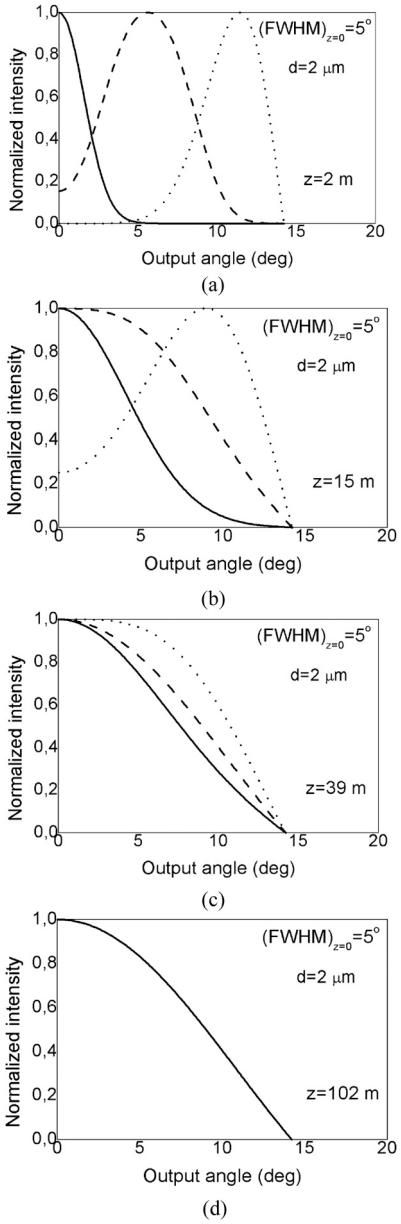

Fig. 3. The evolution of the normalized output angular power distribution with fiber length for the case with $d = 2$ μm calculated for Gaussian input angles $\theta_0 = 0^\circ$ (solid line), 6° (dashed line), and 12° (dotted line) with $(\mathrm{FWHM})_{z=0} = 5^\circ$ for: (a) $z = 2$ m; (b) $z = 15$ m; (c) $z \equiv L_c = 39$ m and (d) $z \equiv z_s = 102$ m.

Table 3
Coupling length L_c (for EMD) and length z_s (for SSD) in SI PPCF with $d = 1$ μm, $d = 1.5$ μm and $d = 3$ μm, for different $(FWHM)_{z=0}$ of the incident beam.

	(FWHM) = 1°		FWHM = 5°		FWHM = 10°	
	L_c [m]	z_s [m]	L_c [m]	z_s [m]	L_c [m]	z_s [m]
$d = 1$ μm	5	13	4.5	12	2.5	6
$d = 1.5$ μm	12.5	31	11	28	9	22
$d = 2$ μm	41	106	39	102	33	85

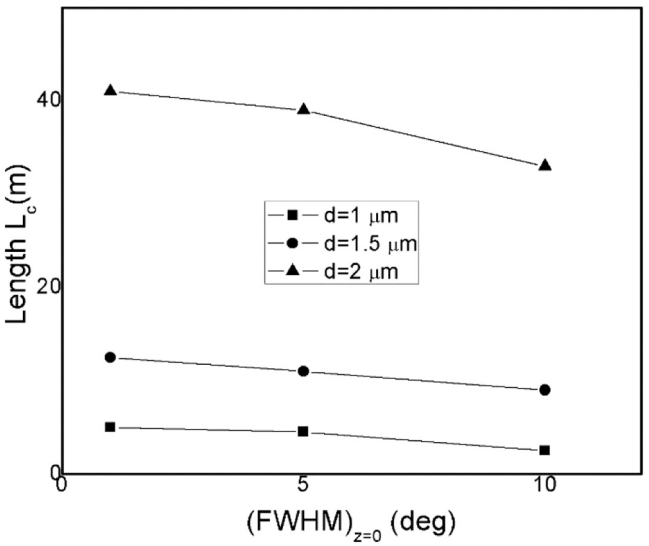

Fig. 4. Length L_c as a function of the launch beam's angular distribution that is Gaussian with $(FWHM)_{z=0} = 1°$, 5° and 10°, for $d = 1$ μm, 1.5 μm and 2 μm.

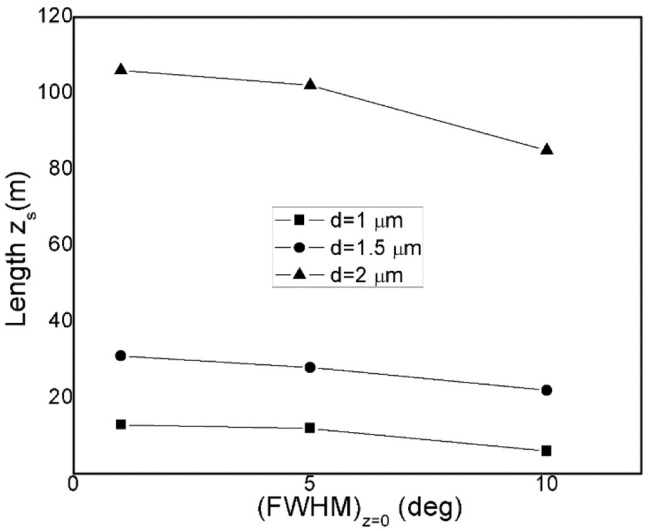

Fig. 5. Length z_s as a function of the launch beam's angular distribution that is Gaussian with $(FWHM)_{z=0} = 1°$, 5° and 10°, for $d = 1$ μm, 1.5 μm and 2 μm.

bandwidth of SI PPCF. Below coupling length L_c the pulse spreading is linear with length. However, beyond this equilibrium length, it has an $L^{1/2}$ dependence. Thus, the shorter the length L_c, the faster bandwidth improvement (slower bandwidth decrease) [39–41].

5. Conclusion

For a multimode step-index plastic photonic crystal fiber with a solid-core and triangular air-hole lattice in the cladding, spatial transients of the power distribution are presented in graph form. These transients are found to be highly dependent on the excitation conditions as well as the size of the air holes in the cladding (NA of the fiber). We obtained that the larger the air holes in the cladding (higher NA), the longer length of the fiber it takes for the modal distribution-transients to reach their equilibrium and steady state. In the case of a wide launch that excites more guiding modes, these lengths shorten. The photonic crystal fibers can be designed with more versatility thanks to these adjustable parameters. Such design flexibility of adjusting structural parameters of the fiber enables dispersion management by affecting the interplay between the material and geometrical dispersions. Dispersion and the resulting mode coupling affect the majority of fiber-based applications.

Declaration of Competing Interest

No conflicts of interests.

Acknowledgements

This work was supported in part by the grant from Serbian Ministry of Education, Science and Technological Development (Agreement No. 451-03-68/2020-14/200122), grant from Science Fund of Republic Serbia (Agreement No. CTPCF-6379382) and by the Strategic Research Grant of City University of Hong Kong (Project No. CityU 7004600).

References

[1] J.C. Knight, T.A. Birks, P. St.J. Russell, D.M. Atkin, All-silica single-mode optical fiber with photonic crystal cladding, Opt. Lett. 21 (1996) 1547–1549.
[2] T.A. Birks, J.C. Knight, P. St J. Russell, Endlessly single-mode photonic crystal fiber, Opt. Lett. 22 (1997) 961–963.
[3] P. St.J. Russell, Photonic crystal fibers, Science 299 (2003) 358–362.
[4] J.C. Knight, Photonic crystal fiber, Nature 424 (14) (2003) 847–851.
[5] P. St.J. Russell, Photonic-crystal fibers, J. Light. Technol. 24 (2006) 4729–4749.
[6] J.C. Knight, J. Broeng, T.A. Birks, P.S.J. Russell, Photonic band gap guidance in optical fibers, Science 282 (1998) 1476–1478.
[7] J.C. Knight, P.S.J. Russell, Photonic crystal fibers: new way to guide light, Science 296 (2002) 276–277.
[8] R.F. Cregan, B.J. Mangan, J.C. Knight, T.A. Birks, P.S.J. Russell, P.J. Roberts, D.C. Allan, Single-mode photonic band gap guidance of light in air, Science 285 (1999) 1537–1539.
[9] R. Amezcua-Correa, F. Gerome, S.G. Leon-Saval, N.G.R. Broderick, T.A. Birks, J.C. Knight, Control of surface modes in low loss hollow core photonic bandgap fibers, Opt. Express 16 (2008) 1142–1149.
[10] G. Bouwmans, L. Bigot, Y. Quiquempois, F. Lopez, L. Provino, M. Douay, Fabrication and characterization of an all-solid 2d photonic bandgap fiber with a low-loss region (<20 db/km) around 1550 nm, Opt. Express 13 (2005) 8452–8459.
[11] F. Luan, A.K. George, T.D. Hedley, G.J. Pearce, D.M. Bird, J.C. Knight, P. St.J. Russell, All-solid photonic bandgap fiber, Opt. Lett. 29 (2004) 2369–2371.
[12] F. Benabid, J.C. Knight, G. Antonopoulos, P. St.J. Russell, Stimulated Raman scattering in hydrogen-filled hollow-core photonic crystal fiber, Science 298 (2002) 399–402.
[13] P.S. Light, F. Benabid, F. Couny, M. Maric, A.N. Luiten, Electromagnetically induced transparency in Rb-filled coated hollow-core photonic crystal fiber, Opt. Lett. 32 (2007) 1323–1325.
[14] D. Mogilevtsev, T.A. Birks, P. St.J. Russell, Group-velocity dispersion in photonic crystal fibers, Opt. Lett. 23 (1998) 1662–1664.
[15] K. Saitoh, M. Koshiba, T. Hasegawa, E. Sasaoka, Chromatic dispersion control in photonic crystal fibers: application to ultra-flattened dispersion, Opt. Express 11 (2003) 843–852.
[16] S. Lee, W. Ha, J. Park, S. Kim, K. Oh, A new design of low-loss and ultra-flat zero dispersion photonic crystal fiber using hollow ring defect, Opt. Commun. 285 (20) (2012) 4082–4087.
[17] D. Chen, M.L.V. Tse, H.Y. Tam, Optical properties of photonic crystal fibers with a fiber core of arrays of sub-wavelength circular air holes: birefringence and dispersion, Prog. Electromagn. Res. 105 (2010) 193–212.
[18] J.K. Ranka, R.S. Windeler, A.J. Stentz, Visible continuum generation in air silica microstructure optical fibers with anomalous dispersion at 800 nm, Opt. Lett. 25 (2000) 25–27.
[19] K.M. Hilligsøe, T.V. Andersen, H.N. Paulsen, C.K. Nielsen, K. Mølmer, S. Keiding, R. Kristiansen, K.P. Hansen, J.J. Larsen, Supercontinuum generation in a photonic crystal fiber with two zero dispersion wavelengths, Opt. Express 12 (2004) 1045–1054.
[20] W.J. Wadsworth, N. Joly, J.C. Knight, T.A. Birks, F. Biancalana, P. St.J. Russell, Supercontinuum and four-wave mixing with Q-switched pulses in endlessly single-mode photonic crystal fibres, Opt. Express 12 (2004) 299–309.
[21] J.H. Lee, W. Belardi, K. Furusawa, P. Petropoulos, Z. Yusoff, T.M. Monro, D.J. Richardson, Four-wave mixing based 10-Gb/s tunable wavelength conversion using a holey fiber with a high SBS threshold, IEEE Photonics Technol. Lett. 15 (2003) 440–442.
[22] T.V. Andersen, K.M. Hilligsøe, C.K. Nielsen, J. Thøgersen, K.P. Hansen, S.R. Keiding, J.J. Larsen, Continuous-wave wavelength conversion in a photonic crystal fiber with two zero-dispersion wavelengths, Opt. Express 12 (2004) 4113–4122.
[23] J. Park, D.E. Kang, B. Paulson, T. Nazari, K. Oh, Liquid core photonic crystal fiber with low-refractive-index liquids for optofluidic applications, Opt. Express 22 (14) (2014) 17320–17330.
[24] S.H. Kassani, R. Khazaeinezhad, Y. Jung, J. Kobelke, K. Oh, Suspended ring-core photonic crystal fiber gas sensor with high sensitivity and fast response, IEEE Photonics J. 7 (2015) 1–9.
[25] W. Wadsworth, R. Percival, G. Bouwmans, J. Knight, T. Birks, T. Hedley, P. St.J. Russell, Very high numerical aperture fibers, IEEE Photon. Technol. Lett. 16 (2004) 843–845.
[26] K.P. Hansen, High-power photonic crystal fibers, in: Proceedings of SPIE, Vol. 6102, pp. 61020B–61020B–11 (SPIE 2006).
[27] K.P. Hansen, C.B. Olausson, J. Broeng, D. Noordegraaf, M.D. Maack, T.T. Alkeskjold, M. Laurila, T. Nikolajsen, P.M.W. Skovgaard, M.H. Sorensen, M. Denninger, C. Jakobsen, H.R. Simonsen, Airclad fiber laser technology, Opt. Eng. 50 (2011), 111609.

[28] R. Stepien, B. Siwicki, D. Pysz, G. Stepniewski, Characterization of a large core photonic crystal fiber made of lead–bismuth–gallium oxide glass for broadband infrared transmission, Opt. Quant. Electron. 46 (2014) 553–561.
[29] M.M. Tefelska, S. Ertman, T.R. Wolinski, P. Mergo, R. Dabrowski, Large area multimode photonic band-gap propagation in photonic liquid-crystal fiber, IEEE Photon. Technol. Lett. 24 (2012) 631–633.
[30] L.V. Amitonova, A. Descloux, J. Petschulat, M.H. Frosz, G. Ahmed, F. Babic, X. Jiang, A.P. Mosk, P. St.J. Russell, P.W.H. Pinkse1, High-resolution wavefront shaping with a photonic crystal fiber for multimode fiber imaging, Opt. Lett. 41 (2016) 497–500.
[31] D. Gloge, Optical power flow in multimode fibers, Bell Syst. Tech. J. 51 (1972) 1767–1783.
[32] M. Rousseau, L. Jeunhomme, Numerical solution of the coupled-power equation in step index optical fibers, IEEE Trans. Microw. Theory Tech. 25 (1977) 577–585.
[33] J. Mateo, M.A. Losada, I. Garcés, J. Zubia, Global characterization of optical power propagation in step-index plastic optical fibers, Opt. Express 14 (2006) 928–935.
[34] K. Saitoh, M. Koshiba, Empirical relations for simple design of photonic crystal fibers, Opt. Express 13 (2005) 267–274.
[35] M.S. Kovačević, Lj Kuzmanović, A. Simović, S. Savović, A. Djordjevich, Transients of modal-power distribution in multimode solid core W-type photonic crystal fibers, J. Light. Technol. 35 (2017) 4352–4357.
[36] S. Savović, A. Djordjevich, Calculation of the coupling coefficient in strained step index plastic optical fibers, Appl. Opt. 47 (2008) 4935–4939.
[37] A.M.R. Pinto, M. Lopez-Amo, Photonic crystal fibers for sensing applications, J. Sens. 2012 (2012) 1–21.
[38] L. Bilro, N. Alberto, J.L. Pinto, R. Nogueira, Optical sensors based on plastic fibers, Sensors 2012 (2012) 12184–12207.
[39] R. Lwin, G. Barton, L. Harvey, J. Harvey, D. Hirst, S. Manos, M.C.J. Large, L. Poladian, A. Bachmann, H. Poisel, K.-F. Klein, Beyond the bandwidth-length product: graded index microstructured polymer optical fiber, Appl. Phys. Lett. 91 (2007), 191119.
[40] A.F. Garito, J. Wang, R. Gao, Effects of random perturbations in plastic optical fibers, Science 281 (1998) 962–967.
[41] D. Richards, A. Lopez, M.A. Losada, P.V. Mena, E. Ghillino, J. Mateo, N. Antoniades, X. Jiang, Overcoming challenges in large-core SI-POF-based system-level modeling and simulation, Photonics 6 (2019) 88.